A Letters Journal Exploring the Frontiers of Physics

August 2007

EPL, **79** (2007) 38004 www.epljournal.org
doi: 10.1209/0295-5075/79/38004

Complex networks in brain electrical activity

C. Ray[1,2], G. Ruffini[1], J. Marco-Pallarés[1,3], L. Fuentemilla[4] and C. Grau[4]

[1] *Starlab Barcelona - Barcelona, Spain*
[2] *Department of Physics, Saint Mary's College - Moraga, CA, USA*
[3] *Department of Neuropsychology, Otto von Guericke Universität-Magdeburg - Germany*
[4] *Neurodynamics Laboratory, Department of Psychiatry and Clinical Psychobiology, University of Barcelona - Spain*

received 5 January 2007; accepted in final form 19 June 2007
published online 16 July 2007

PACS 87.18.Sn – Neural networks
PACS 87.19.Nn – Electrophysiology
PACS 89.75.-k – Complex systems

Abstract – This letter reports a method to extract a functional network of the human brain from electroencephalogram measurements. A network analysis was performed on the resultant network and the statistics of the cluster coefficient, node degree, path length, and physical distance of the links, were studied. Even given the low electrode count of the experimental data the method was able to extract networks with network parameters that clearly depend on the type of stimulus presented to the subject. This type of analysis opens a door to studying the cerebral networks underlying brain electrical activity, and links the fields of complex networks and cognitive neuroscience.

Introduction. – Functional magnetic resonance imaging (fMRI) data for the human brain has been analyzed [1] using a complex networks approach, and evidence was found for a scale-free behavior of the derived functional networks. The spacial resolution of fMRI is outstanding, less than $1\,\mathrm{cm}^3$, but the temporal resolution is fundamentally limited, because fMRI measures the metabolic activity of the brain, through the blood oxygen level difference. Because the metabolic activity is a temporal convolution of the computational activity, the temporal resolution is at best on the order of a second. EEG signals on the other hand, with a temporal resolution of less than a milliseconds, are a measure more directly related to the computational activity of the brain neural ensemble dendritic currents, reflecting excitatory-inhibitory neural communication processes which are believed to reveal the effective network of the brain [2]. Hence, EEG allows recording real-time synchronous neural activity which closely link neural computing and behavior [3]. However, while EEG signals seem to be very rich in information, reliable extraction of information has been elusive [4]. A particular difficulty for using EEG's to study the functional network of the brain is the fact that EEG signals are only measured at the electrodes on the scalp. So that, until now, only the network derived from the connectivity of the surface electrode signals has been studied [5], which does not reveal the network between the functional regions of the brain. However, with recent advances in EEG tomography [6] it is now possible to locate the source of the signals within the brain, with course accuracy. This development makes possible the construction of functional networks of the brain with a much greater temporal resolution, by a combination of EEG tomography and the methodology employed in [1]. In this paper we describe such a "complex networks" methodology for electrophysiology and apply it to a relatively simple set of data obtained in an event-related potential protocol with 13 subjects and collected with 30 EEG channels. While it is certainly true that 30 electrodes are barely sufficient to obtain good tomographic results, the aim here is to carry out a first test of the approach. The technique can be applied with more extensive data sets, and the envisioned applications are many.

Experimental procedure. – In this work we have applied our analysis to a set of previously obtained and well-studied data. It is a widely observed phenomena in psychophysiology that when a novel (deviant) tone appears in a background of similar (standard) stimuli, the cerebrum elicits an electrical response that peaks 100–200 ms after the deviant stimulus, even if the subject is not attending to the stimuli. This response can be recorded, using EEG, as a negative voltage at the frontocentral electrodes. This negative wave is known as Mismatch Negativity (MMN). The paradigm used in

collecting the data, described fully in [7,8], was designed to study this process. The stimuli were auditory and consisted of pure sine-wave tones (700 Hz), with a duration of either 75 ms (standard) or 25 ms (deviant). Trains of three tones at intervals of 300 ms were presented to subjects. The first tone of each train was either standard or deviant with equal probability, while the second and third tones were always standard. The analysis performed in this study utilized epochs of 400 ms of EEG data that started 100 ms before the first tone. For each subject 100 standard and 100 deviant trials were analyzed.

Sixteen healthy subjects (mean age 39 ± 11 years) participated in the study. Three subjects were excluded from the rest of the study because they did not have an identifiable mismatch negativity wave [9]. The subjects were instructed to ignore auditory stimuli while they performed an unrelated visual task. In what follows, electrode voltage time series will be identified by $\phi_q(t_i)$, where the q index refers to the electrode number, and t_i to the time of sampling events.

Computation of network from EEG data. – The network is constructed from the EEG data in three steps. First, Low-Resolution Tomography (LORETA) [6] is employed to estimate the current densities within the brain from the measured electrode voltages on the scalp. LORETA is an L2 minimum normalization that solves the inverse problem of EEG, that is it estimates the current sources within the brain that produce the measured EGG voltages at the scalp. Because the inverse is not unique, this problem is not well defined. LORETA finds the inverse that produces the source current density with the smoothest spacial variation. In the past five years, this tomographic approach has been used in several neuroscience studies, *e.g.* [8,10–13]. The result of the LORETA algorithm is a linear transformation (T_{nq}) which computes the estimated current densities ($\tilde{J}_n$) at distinct location (voxels) within the Talairach human brain [6] from the electrode voltages (ϕ_q):

$$\tilde{J}_n = \sum_q T_{nq}\phi_q.$$

The "activation" of a voxel is defined to be the magnitude of the (vector) current density,

$$I_n = ||\tilde{J}_n|| = ||\sum_q T_{nq}\phi_q||. \tag{1}$$

For each time step of each trial, for each subject, the electrode data is transformed into a voxel activation level using LORETA, producing 2394 voxel activation time series $I_n(t_i)$ for each trial, for each subject.

The second step is the computation of the inter-voxel correlation coefficient. The correlation coefficient c_{nm} between voxels n and m for a single trial, is defined to be the correlation coefficient of the activations over time:

$$c_{nm} = \frac{\langle I_n I_m\rangle_t - \langle I_n\rangle_t\langle I_m\rangle_t}{\sigma_n\sigma_m} = \langle S_n S_m\rangle_t, \tag{2}$$

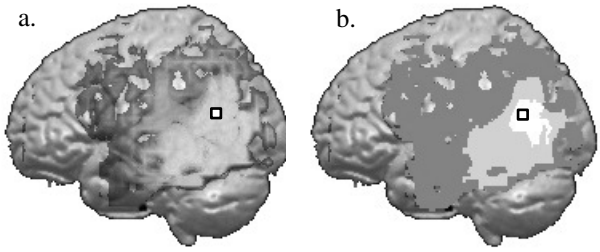

Fig. 1: The thresholding process is represented in this figure. In (a) the magnitude of the correlation coefficient between the voxel marked with a small square and other voxels is represented by a grayscale. In (b) the regions connected to the voxel are shown at three different thresholds. The white region is the region connected at a large threshold, while the light grey shows the region connected at a medium threshold, and the dark grey is the region connected at a small threshold.

where $\langle\cdots\rangle_t$ denotes a time average, $\sigma_n^2 = \langle I_n^2\rangle_t - \langle I_n\rangle_t^2$, and $S_n(t_i) = [I_n(t_i) - \langle I_n\rangle_t]/\sigma_n$ is the demeaned and normalized activation signal. The activation correlation coefficient used here is defined to be the average of c_{nm} over all 100 trials. The notation $\bar{c}_{nm}$will be used for the average activation correlation coefficient matrix.

The third step is to determine which voxels are linked. When the absolute value of the correlation between voxels n and m is greater than a chosen threshold r_c, the voxels are linked, otherwise the voxels are not linked (as in [1]). This process is represented in fig. 1. This defines the connectivity matrix, with entries equal to 1 (voxels are linked) or 0 (not linked),

$$A_{nm} = \begin{cases} 1, \text{ if } |\bar{c}_{nm}| > r_c \text{ and } n \neq m, \\ 0, \text{ otherwise.} \end{cases} \tag{3}$$

In the data set that is analyzed here, a network is constructed for each subject for both deviant and standard conditions and for six different threshold. This gives a total of 156 networks.

Network analysis. – Once a network is defined by the connectivity matrix, it is possible to study measures associated with the network [1,14]. The following measures are computed for the network. The notation $\langle\cdots\rangle$ indicates an average over the nodes or links of a single network.

- N, is the number of nodes with at least one link. This measure deviates less than 1% from the maximum (2394) for all networks studied.

- k_n is the degree of node n, the number of nodes linked to node n:

$$k_n = \sum_i A_{ni} = \sum_i A_{ni}A_{ni} = \sum_i A_{ni}A_{in} = A^2_{nn}, \qquad \langle k\rangle = \frac{1}{N}\sum_n k_n = \frac{1}{N}\mathrm{Tr}[A^2]. \tag{4}$$

– C_n is the cluster coefficient for node n, the ratio of the number of links between the neighbors of node n and the maximum possible number of links between the neighbors. With $\nu_n = \{m|A_{nm} = 1\}$, the set of neighbors of node n, the cluster coefficient can be written as follows:

$$C_n = \frac{\sum_{i,j\in\nu_n} A_{ij}}{k_n(k_n-1)} = \frac{A^3_{nn}}{k_n(k_n-1)}. \qquad (5)$$

Note that the second form is equivalent because the restricted sum of A_{ij} is the same as the unrestricted sum of $A_{ni}A_{ij}A_{jn}$, since either A_{ni} or A_{jn} is zero for the added elements of the sum and both are 1 for the original elements of the sum. $\langle C\rangle$ is the average cluster coefficient, an indicator of the fraction of completed sub-networks. For an equivalent random network $\langle C\rangle = \langle k\rangle/(N-1)$.

– L_{nm} is the path length between nodes n and m, the minimum number of links required to travel through the network from node n to node m. $\langle L\rangle$ is the average path length, the average is computed over all pairs of nodes that are linked by a path, unlinked pairs are excluded from the average. L_{max} is the maximal path length (the network perimeter). For a random network it is approximated by $L_{max} = \ln N/\ln\langle k\rangle$ [15].

– $\langle d\rangle$ is the average physical length of the links, measured in mm. This is not a topological measure but relevant nonetheless in the present study.

Because of the smoothing caused by the tomography, nearest (physical distance) neighbors are almost universally connected, at all thresholds. Thus there is essentially only one component (group of connected nodes) in all cases. At the highest threshold, there would be a few voxels that were disconnected from the main component, but even at a threshold of 0.9, less than 0.4% of the nodes were disconnected from the main component.

The average over all subjects ($\langle\cdots\rangle_s$), of the network parameters for various thresholds and both deviant and standard conditions are graphed in fig. 2. The standard deviation of the parameters was also computed to provide a measure of the variation of these parameters over subjects. For comparison, the parameters that are found for a simulated EEG signal, composed of uncorrelated electrode signals, are graphed along with the experimental results. This choice of reference signal is discussed more fully in the following section. Because it is a commonly used reference, the values of the cluster coefficient and average path length for random networks with an equal number of links, are also graphed. In this case, the uncorrelated electrode signal reference is more useful, since it represents the parameters that result from a null signal.

Estimation of correlations induced by the tomographic inverse transformation. – The tomographic processing induces artificial correlations in the voxel activations. In our test data set there were 30 electrode signals and 2394 voxel signals. The voxel signals are a linear combination of the electrode signals, and thus the voxel signals must be linearly dependent. For this reason there will be correlations in the voxel activations even if the electrode data is randomly generated and fully uncorrelated.

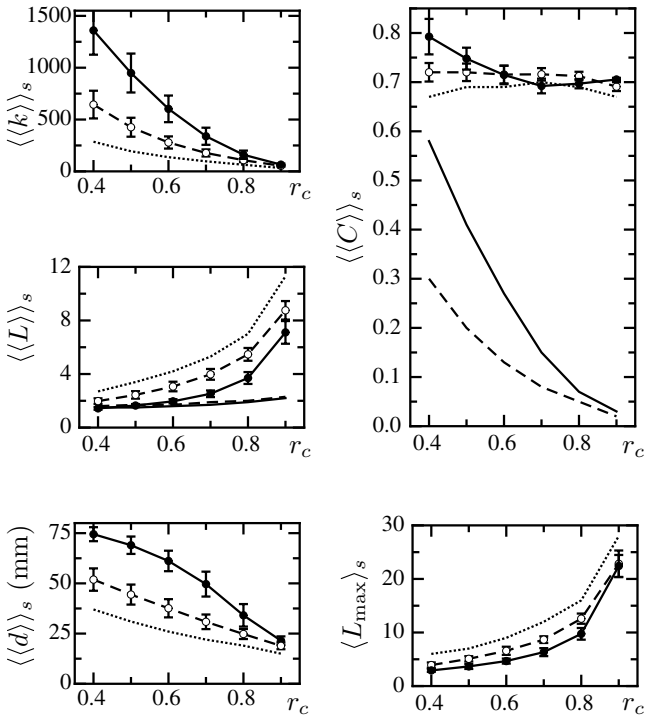

Fig. 2: Subject average of the network parameters as a function of correlation threshold: solid is standard, dashed is deviant. The error bars reflect the standard deviation of the values. The dotted line is the parameters that results from random uncorrelated electrode signals. In the $\langle C\rangle$ and $\langle L\rangle$ graphs, the solid and dashed lines without data points are the parameters for random networks with an equal number of links to the standard and deviant networks.

It is possible to work with up to 256 electrodes, and this will certainly increase the effective tomographic resolution. In addition the LORETA tomographic method uses an L2 minimum norm, which leads to a very smooth current field. The use of other methods could reduce the induced correlations. Nevertheless, even with 256 electrodes and improved tomographic methods, the tomography induced correlations will persist, so a thorough analysis of this effect is needed. Here we provide only an estimate of the magnitude of the effect of the tomography-induced correlations on the network. The tomography-induced correlations can be estimated by computing the correlations induced by the tomography when the electrode data is fully uncorrelated. This measure is also relevant to the analysis of the impact of uncorrelated noise at the electrodes. The network parameters that results from uncorrelated electrode data are graphed in fig. 2. The network

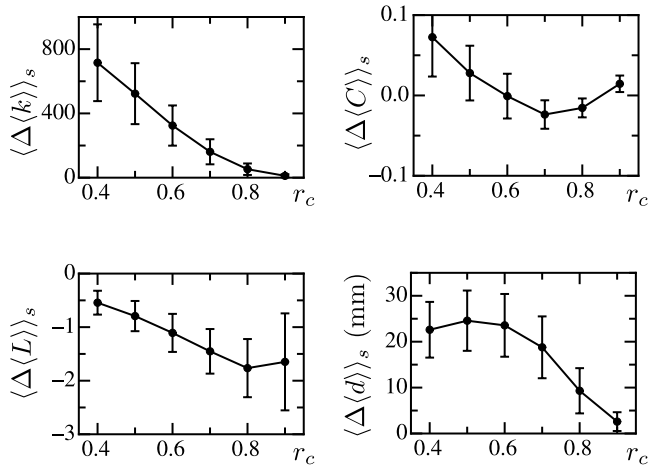

Fig. 3: Subject average of the difference between the standard and deviant network measures, as a function of correlation threshold. For example, the subject average of the difference for the degree parameter was computed as follows: $\langle\Delta\langle k\rangle\rangle_s = \langle\langle k\rangle^{\text{standard}} - \langle k\rangle^{\text{deviant}}\rangle_s$. The error bars reflect the standard deviation of the subject average. It can be seen in these graphs that the difference is distinguishable from zero for $\langle k\rangle$, $\langle L\rangle$ and $\langle d\rangle$. while $\langle C\rangle$ is indistinguishable from zero.

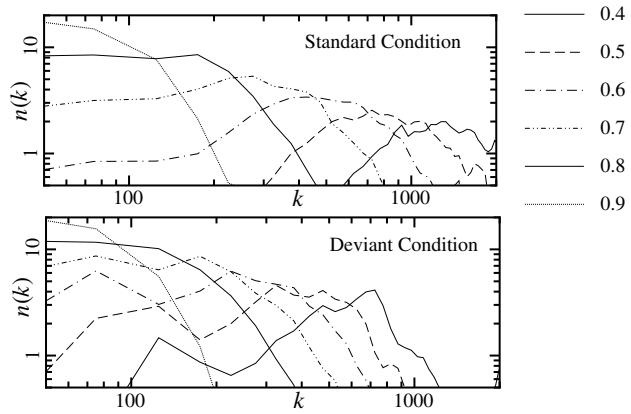

Fig. 4: This is a log-log graph of the degree distribution averaged over all subjects, for cutoffs from $r_c = 0.4$ to $r_c = 0.9$.

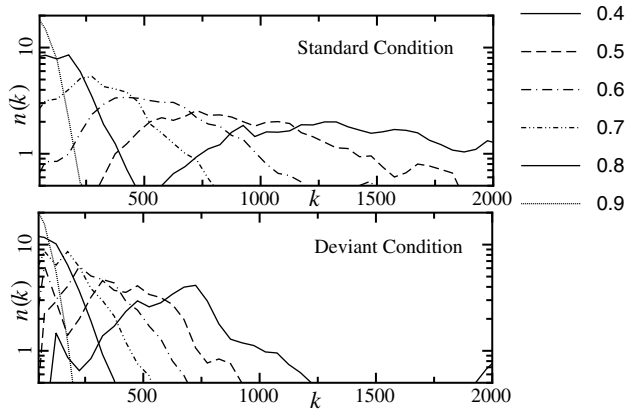

Fig. 5: This is a log-linear graph of the degree distribution averaged over all subjects, for cutoffs from $r_c = 0.4$ to $r_c = 0.9$.

parameters for the actual signals should be viewed relative to this reference point established by the uncorrelated signals.

Differences between stimulus conditions. – In fig. 2 it can be seen that the average network parameters, $\langle k\rangle$, $\langle L\rangle$ and $\langle d\rangle$ for the standard and deviant networks are significantly different from each other and from the background. The cluster coefficient does not appear to be a significantly different. To clarify the statistical significance of these differences, and to show that the differences exists for each individual subject, the subjects average of the differences of the average parameters for the standard and deviant networks were computed. For example, the difference for the degree parameter was computed as follows:

$$\langle\Delta\langle k\rangle\rangle_s = \langle\langle k\rangle^{\text{standard}} - \langle k\rangle^{\text{deviant}}\rangle_s.$$

These results are graphed in fig. 3. It can be seen in these graphs that the difference is distinguishable from zero for $\langle k\rangle$, $\langle L\rangle$ and $\langle d\rangle$. While $\langle C\rangle$ is indistinguishable from zero. This indicates that $\langle k\rangle$, $\langle L\rangle$ and $\langle d\rangle$ have potential as biometric measures.

The cluster coefficient is nearly constant over the range of thresholds studied, see fig. 2. In addition the cluster coefficient for the uncorrelated electrodes is almost as large. It is suspected that the correlations cause by the tomography have in some sense flooded the cluster coefficient.

Scale-free behavior. – In fig. 4 and fig. 5 the average degree distribution, $n(k)$, is graphed. The function $n(k)$ is the average number of nodes with degree k. The average is computed over trials and subjects. Figure 4 is a log-log graph, and thus if $n(k)$ is a power of k it will appear as a straight line in fig. 4. Such a power law behavior is associated with a scale-free network. In contrast fig. 5 is a log-linear graph, and thus if $n(k)$ is an exponential in k it will appear as a straight line in fig. 5. While neither the log-log nor the log-linear graphs are linear, the log-linear is closer to being straight. In this way our results are similar to those in [16–18], in which the networks were not found to be scale free, and different from those in [1].

Conclusion. – In this letter we have reported a preliminary study of a method to extract a connectivity network representing brain interactivity from the brain electrical activity as observed through EEG measurements. We have found that, even with the limited spacial resolution of the tomography, the networks generated from brain activity under two different stimuli were distinguishable by their network parameters. The change in the network parameters with stimulus, was statistically significant and stable across subjects and at different correlation

thresholds. There is not a clear indication that the networks are scale free.

The application of this approach could range from the basic studies determining the properties of networks associated with event-related potentials or electroencephalography, to the study of pathological brain electrical responses, to biometrics. However, more studies are needed in order to compare the information provided by an electrophysiology complex networks approach with information provided by other functional techniques, such as fMRI, and theoretical information to clearly validate this method. In particular, we plan to analyze elsewhere in more detail the impact of the tomography on the network structure, as well as study other variants for the construction of the networks.

* * *

This work has been partly funded by the Starlab Kolmogorov program under the auspices of the FURNET network. GR would like to thank E. Rietman for valuable discussions, and in particular for pointing out the relevance of [1]. The authors wish to acknowledge support received from the Generalitat of Catalonia NECOM group (SGR2005-00831), the Spanish Ministry of Culture and Education (SEJ2006-13998), the EU FP6 Sensation Integrated Project (FP6-507231), and Macken Instruments. Finally, the authors thank C. Escera and M. Dolores Polo (U. Barcelona) for data collection.

REFERENCES

[1] Eguíluz V. M. *et al.*, *Phys. Rev. Lett.*, **94** (2005) 018102.
[2] Bressler S. L., *The handbook of brain theory and networks* (MIT Press, Cambridge, MA) 2002.
[3] Buzsaki G. and Draguhn A., *Science*, **304** (2004) 1926.
[4] Nunez P. L., *Neocortical Dynamics and Human EEG Rhythms* (Oxford University Press, New York) 1995.
[5] Stam C. J. *et al.*, *Cereb. Cortex*, **17** (2007) 92.
[6] Pascual-Marqui R. D., Michel C. M. and Lehmann D., *Int. J. Psychophysiol.*, **18** (1994) 49.
[7] Grau C., Escera C., Yago E. and Polo M. D., *Neuroreport*, **9** (1998) 2451.
[8] Marco J., Grau C. and Ruffini G., *Neuroimage*, **25** (2005) 471.
[9] Näätänen R., *Attention and brain function* (Lawrence Erlaum Associates Publishers, Hillsdale, New Jersey) 1992.
[10] Gomez C., Marco J. and Grau C., *Neuroimage*, **20** (2003) 216.
[11] Kounios J. *et al.*, *Neuron*, **29** (2001) 297.
[12] Mulert C. *et al.*, *Neuroimage*, **13** (2001) 589.
[13] Pizzagalli D. *et al.*, *Am. J. Psychiatry*, **158** (2001) 405.
[14] Albert R. and Barabasi A. L., *Rev. Mod. Phys.*, **74** (2002) 47.
[15] Fronczak A., Fronczak P. and Holyst A., *Phys. Rev. E*, **70** (2004) 056110.
[16] Hilgetag C. C. *et al.*, *Philos. Trans. R. Soc. London, Ser. B Biol. Sci.*, **355** (2000) 91.
[17] Salvador R. *et al.*, *Cereb. Cortex*, **15** (2005) 1332.
[18] Scannell J. W. *et al.*, *Cereb. Cortex*, **9** (1999) 277.